Nuclear Magnetic Resonance Studies of the N-Terminal Fragment of Adenosine Diphosphate Ribosylation Factor 1 in Micelles and Bicelles: Influence of N-Myristoylation†

Judit A. Losonczi,‡ Fang Tian, and James H. Prestegard*

Complex Carbohydrate Research Center, University of Georgia, 220 Riverbend Road, Athens, Georgia 30602-4712

Received October 5, 1999; Revised Manuscript Received January 10, 2000

ABSTRACT: The N-terminal fragment of adenosine diphosphate (ADP) ribosylation factor 1 (ARF1) is proposed to be involved in the guanosine triphosphate- (GTP-) dependent, reversible association of the protein with membranes through the interaction of not only the N-linked myristoyl chain but also its highly conserved N-terminal hydrophobic residues. Based on the N-terminal sequence of this protein, specifically ^{13}C- and ^{15}N-labeled peptides were synthesized with and without an *N*-myristoyl anchor. The behavior, including structure, dynamics, and orientation, of these peptides in a lipid environment was then studied through a combination of solution ^{1}H nuclear magnetic resonance (NMR) techniques in micelles and heteronuclear solid-state NMR experiments in magnetically aligned bicelles. The work presented is an extension of the previously reported characterization of the myristoylated N-terminal fragment of ARF1 [Losonczi and Prestegard (1998) *Biochemistry 37*, 706−716] to include a comparison to a nonmyristoylated analogue. Results indicate that both myristoylated and nonmyristoylated peptides are α-helical in a lipid environment and that N-myristoylation does not greatly influence the structure of the peptides. Evidence is presented suggesting association of the peptides with bilayer disks through a combination of edge and surface interactions.

A large number of cellular processes are organized at the membrane surfaces of cells. Proteins participating in these processes are often integral membrane proteins, but they can also be more loosely associated proteins interacting with the aid of one or more lipid-derived anchors (*1*, *2*). The *N*-myristoyl lipid chain is one of the most commonly occurring lipid modifications of proteins (*3*). These *N*-myristoyl proteins have diverse biological functions. Examples include the adenosine diphosphate ribosylation factors of the guanosine triphosphatase superfamily, protein kinases such as the catalytic subunit of cyclic adenosine monophosphate-dependent protein kinase, the gag polyprotein precursor of human immunodeficiency virus type 1 (HIV-1), the Ca^{2+} sensor, recoverin, and the α-subunit of G proteins. In most of these cases the lipid modification is believed to be essential for reversible protein−membrane interaction, although it is suggested that the hydrophobic interaction of the myristoyl lipid chain with membranes is not sufficient to anchor most proteins to the bilayer, and additional factors need to be considered. Such factors could be electrostatic interactions of basic protein residues with acidic phospholipids or the hydrophobic interaction of an amphipathic helix of the protein with the bilayer (*4*). It has also been shown that N-myristoylation can play a role in protein−protein interactions (*5*), raising further questions as to the exact role a lipid anchor may play in protein function.

We present here structural work relevant to the roles of N-myristoylation and the N-terminal amphipathic helix for a protein important in membrane trafficking, ADP ribosylation factor 1 (ARF1)[1] (*6*). The experiments conducted employ NMR methodology dependent on the field-induced orientation of lipid bilayer arrays with which the protein associates. In addition to returning useful data on the ARF protein, the experiments lay groundwork for future applications to other proteins where the nature of membrane−protein association is at issue.

Even though N-myristoylated proteins and peptides are of great interest and importance, to date only a few have been studied in a lipid environment, and no structural study addresses the specific role and effect of the lipid anchor. There is a detailed solution structure of the N-myristoylated recoverin molecule (*7*) and the anchor domain of the HIV-1 Nef protein (*8*), but no structures in the presence of even

† This work was supported by NIH Grant GM54160.

* To whom correspondence should be addressed.

‡ Present address: Abbott Laboratories, 100 Abbott Park Rd., D-47G, AP10, Abbott Park, IL 60064-6098.

[1] Abbreviations: ARF, adenosine diphosphate (ADP) ribosylation factor; ARF1-Myr15, Myr-GNIFANLFKGLFGKK; ARF1-15, GNIFANLFKGLFGKK; CP, Hartmann−Hahn cross polarization; CSA, chemical shift anisotropy; DHPC, L-α-dihexanoylphosphatidylcholine; DPC, dodecylphosphocholine; DMPC, L-α-dimyristoylphosphatidylcholine; DMSO, dimethyl sulfoxide; DQF-COSY, double quantum filtered correlation spectroscopy; DSS, 2,2-dimethyl-2-silapentane-5-sulfonate, sodium salt; EPR, electron paramagnetic resonance; FSLG, frequency-switched Lee−Goldburg homonuclear decoupling; GDP, guanosine diphosphate; GTP: guanosine triphosphate; INADEQUATE, incredible natural abundance double quantum transfer experiment; INEPT, insensitive nuclei enhanced by polarization transfer; NMR, nuclear magnetic resonance; LPC, lysophosphatidylcholine; NOESY, nuclear Overhauser effect spectroscopy; PAF, principal averaging frame or principal axis frame; SLF, separated local field experiment; SVD, singular value decomposition; TOCSY, total correlation spectroscopy.

10.1021/bi9923050 CCC: $19.00
Published on Web 03/09/2000

Table 1: Labeling Patterns for the ARF1-Myr15 and the ARF1-15 Peptides

name	labeling pattern
ARF1-Myr15-I	[1,2-$^{13}C_2$]Myr[^{15}N]GlyAsnIlePheAlaAsn[1,2-$^{13}C_2$]Leu$_8$[^{15}N]Phe$_9$Lys[1,2-$^{13}C_2$]Gly$_{11}$[1,2-$^{13}C_2$]Leu$_{12}$[^{15}N]Phe$_{13}$GlyLysLys
ARF1-Myr15-II	MyrGlyAsnIlePheAlaAsnLeu[*ring*-$^{13}C_6$]Phe$_9$LysGly[1,2-$^{13}C_2$]Leu$_{12}$[^{15}N]Phe$_{13}$GlyLysLys
ARF1-Myr15-III	MyrGlyAsn[1-^{13}C]Ile$_4$[^{15}N]Phe$_5$AlaAsn[^{15}N]Leu$_8$ PheLysGlyLeu[*ring*-$^{13}C_6$]Phe$_{13}$GlyLysLys
ARF1-Myr15-IV	MyrGlyAsnIle[*ring*-$^{13}C_6$]Phe$_5$AlaAsn[^{15}N]Leu$_8$PheLys[1-^{13}C]Gly$_{11}$[^{15}N]Leu$_{12}$PheGlyLysLys
ARF1-15-I	[1,2-$^{13}C_2$]GlyAsnIle[^{15}N-56%]Phe$_5$AlaAsn[1,2-$^{13}C_2$]Leu$_8$[^{15}N]Phe$_9$Lys[1,2-$^{13}C_2$]Gly$_{11}$[1,2-$^{13}C_2$]Leu$_{12}$[^{15}N]Phe$_{13}$[^{15}N]Gly$_{14}$LysLys
ARF1-15-II	GlyAsnIlePheAlaAsnLeu[*ring*-$^{13}C_6$]Phe$_9$LysGly[1,2-$^{13}C_2$]Leu$_{12}$[^{15}N]Phe$_{13}$GlyLysLys

model membrane systems, such as detergent micelles or phospholipid bilayer vesicles, are available. Studies on the interaction of short, N-myristoylated peptides with lipid bilayers have been conducted by EPR (*9*) and ^{2}H NMR spectroscopy (*10*) but with focus on the lipid anchor itself, not the peptide. EPR spectroscopy of selectively spin-labeled membrane associated basic peptides has also been used to study electrostatic and hydrophobic interactions between the peptides and lipid vesicles (*11*, *12*). These studies yield information on approximate locations of the spin labels relative to the bilayer interface but cannot give a detailed structural model.

The peptides to be studied here are derived from the N-terminus of ARF1, a relatively small (21 kDa) protein that plays an important role in membrane trafficking by controlling the assembly and disassembly of transport vesicle coats (*13*, *14*). The inactive GDP-bound form of ARF is cytosolic, whereas the GTP-bound form of ARF binds to lipid bilayers in a myristate- and GTP-dependent manner. While both the N-myristoylated ARF_{GDP} and the unacylated ARF_{GTP} bind weakly to lipid vesicles, the unmyristoylated ARF_{GDP} shows no binding at all (*15*, *16*). D17-ARF1, a mutant lacking the lipid chain and the first 17 residues, also loses the ability to bind to lipids and remains soluble whatever the bound nucleotide (*17*).

ARF1 has 21% sequence identity and some similarity in the fold of the protein core to Ras p21, but its N-terminal helix and loop have no counterpart in the Ras family. The sequence of this N-terminal segment suggest that it folds into an amphipathic helix and is likely to be the protein domain responsible for the GTP-dependent binding of the protein to bilayers. This N-terminal sequence, especially the amphipathic pattern, is highly conserved in all six human ARF proteins. The X-ray structure of the nonmyristoylated, GDP-bound form of ARF1 is known (*18*) as well as the crystal structure of D17-$ARF1_{GTP}$, a mutant lacking the first 17 N-terminal amino acids (*19*). In the X-ray structure of $ARF1_{GDP}$, the N-terminal segment of the protein is a helix, up to residue 11, and it is held in a groove of the protein by hydrophobic forces. Comparison to the structure of D17-$ARF1_{GTP}$ has led to a preliminary model of how nucleotide exchange might lead to helix and fatty acid exposure (*19*). It has also been suggested that the N-terminal α-helix might extend further in the membrane-bound form than in the water-soluble form (beyond residue 11), so that all conserved hydrophobic residues can make contact with the membrane (*18*).

The existence of two participants in membrane interaction, the lipid chain, which gives a basal affinity for lipids regardless of the protein conformation, and a protein region that becomes available for membrane binding only when they are switched to the active, GTP-bound form, has a great deal of appeal in explaining biochemical data (*20*−*22*). However, confirming hypotheses relating to the nature of myristoylated helix interactions with a membrane is only possible by studying ARF1 systems in a bilayer environment. NMR spectroscopy applied in micelles and bicelles, even to isolated terminal sequences of ARF1, can contribute to this study.

One possibility for the study of membrane−protein interactions is to use detergent micelles to mimic a membranelike environment. Peptides and proteins in these systems reorient fast enough to give sufficient resolution for multidimensional solution NMR experiments and traditional NOE-based structural determinations (*23*, *24*). While the small spherical micelles yield high resolution, magnetically aligned bilayer disks, composed of short- and long-chain phospholipids, offer the opportunity to extend studies of lipid-modified peptides to an environment that more closely resembles the planar surface of biological membranes (*25*). Moreover, these bilayer disks, often referred to as bicelles, show homogeneous alignment with respect to the magnetic field, making possible the determination of peptide orientation relative to a bilayer surface.

We have previously reported on the NMR characterization of the myristoylated N-terminal fragment of the ADP-ribosylation factor 1 (ARF1-Myr15) in bicelles (*26*) using a minimal set of NMR data relating to the peptide backbone structure. To extend this study, the nonmyristoylated form of this fragment has now been synthesized and studied both by high-resolution ^{1}H NMR in micelles and by heteronuclear solid-state NMR techniques in magnetically aligned bicelles. New N-myristoylated peptides (ARF1-Myr15) have also been synthesized and studied. There has been one change in previously reported resonance assignments for the myristoylated peptide, but the overall backbone structure remains the same. More importantly, results indicate that both myristoylated and nonmyristoylated amphipathic peptides form a helix upon interaction with lipids and that the N-myristoylation, while enhancing binding, does not affect the peptide structure or behavior to a significant degree.

MATERIALS AND METHODS

Peptides. Four myristoylated 15 amino acid peptides (ARF1-Myr15, MGNIFANLFKGLFGKK) were synthesized that differ only in the isotopic labeling pattern. In all, labels were introduced across five amide bonds by incorporating ^{13}C carboxyl, and sometimes $^{13}C_\alpha$, labels in the N-terminal partner in the bond and an amide ^{15}N label in the C-terminal partner in the bond. Table 1 summarizes the labeling patterns. Labeled amino acids and [1,2-$^{13}C_2$] myristic acid were purchased from Isotec Inc. (Miamisburg, OH). The Fmoc-protected labeled amino acids were synthesized according to standard procedures (*27*) and supplied to the Keck Biotechnology Laboratory at Yale University for solid-phase synthesis and column purification (50 μM scale, ∼30% yield).

The nonmyristoylated 15 residue peptides (ARF1-15, GNIFANLFKGLFGKK) were synthesized on an Applied Biosystems 431A peptide synthesizer by a standard, small-scale (0.1 mM), solid-phase peptide synthesis technique with Fmoc-protected amino acids and HBTU [2-(1*H*-benzotriazol-1-yl)-1,1,3,3-tetramethyluronium hexafluorophoshate) activation. The peptides were purified by reverse-phase HPLC on a Vydac C18 preparative column. Typical yields were ~40%. Two forms of the nonmyristoylated peptides were synthesized, differing only in the labeling pattern (Table 1).

High-Resolution ^{1}H NMR in Micelle Solutions. The micellar samples were prepared with a detergent (dodecylphosphocholine-d_{38}, Cambridge Isotope Laboratories, Inc.) concentration of 40−50 mM and a peptide concentration of 2 mM for ARF1-15 and 3.6 mM for ARF1-Myr15, in a 15% D_2O solution of pH 7, 20 mM Bis-Tris buffer. The typical lipid:peptide ratio was 15−30:1; increasing this ratio had no effect on the NMR spectra.

NMR experiments were recorded at 45 °C on a 600 MHz Varian Inova spectrometer equipped with a 5 mm ^{1}H/^{13}C/^{15}N indirect detect probe and a *z* axis pulsed-field gradient accessory. The following experiments were executed: one-dimensional ^{1}H, DQF-COSY (*28*), TOCSY (*29*) (with presaturation for water suppression), and NOESY (*30*) (using pulsed field gradients for water suppression, (*31*). The TOCSY mixing time was 60 ms, and the NOESY mixing time was 150 ms. Typical experimental parameters include a 6.9 μs 90° pulse width, 256 ms acquisition time, and 8000 Hz sweep width (2048 complex t_2 points). Four hundred complex t_1 points were acquired, 16 scans at each increment with a 1 s delay after scans. The spectra were referenced to DSS (*32*).

High-Resolution ^{13}C and ^{15}N NMR in Micelle Solutions. An isotropic micelle phase was also prepared from lysophosphatidylcholine (LPC; Avanti Polar Lipids, Birmingham, AL) to provide a chemical shift reference for the measurement of the anisotropic contribution to the carbonyl ^{13}C and the amide ^{15}N chemical shift (δ_{an}). For these isotropic micelle samples ARF1-Myr15 and ARF1-15 were reconstituted into LPC micelles by simple mixing (0.25 mM LPC solution with LPC:peptide ratio of around 100:1). The ^{13}C spectra were collected at 45 °C in a simple one-pulse experiment with NOE enhancement, and the ^{15}N spectra were collected by use of the INEPT sequence for enhancement, also at 45 °C.

Bicelle Preparation. Bicelle samples were prepared by a method previously described (*33*, *34*), and characterized by ^{31}P NMR to assess the degree of order (*25*, *26*). DMPC (L-α-dimyristoylphosphatidylcholine) was purchased from Sigma (St. Louis, MO). DHPC (L-α-dihexanoylphosphatidylcholine) was purchased from Avanti Polar Lipids (Birmingham, AL). The typical lipid composition used was DMPC:DHPC 2.8:1 mole ratio, 25% (w/v) total amphiphile. All bicelle samples were buffered at pH 7 with a low total buffer and salt concentration of 20 mM to avoid heating effects during the high-power decoupling periods. For ARF1-Myr15, the typical lipid:peptide mole ratio was 60−100:1; ARF1-15 was easily incorporated into bicelles at peptide to lipid molar ratios similar to ARF1-Myr15.

Solid-State NMR Spectroscopy. Most of the data were collected on a 500 MHz Varian Inova spectrometer equipped with a triple-resonance ^{13}C and ^{15}N detector 5 mm high-resolution solution probe from Nalorac Corp. The probe was specifically modified to handle higher power on the proton channel for extended periods of time (30 W up to 30 ms). Carbon-13 chemical shifts were referenced externally to dioxane at 69.2 ppm, and nitrogen-15 chemical shifts were referenced to ^{15}N ammonium nitrate at 21 ppm. The ^{13}C spectra of carbonyl carbons were recorded in a one-pulse experiment with nuclear Overhauser enhancement. Typical experimental parameters were 1−2 s saturation times, 10 μs ^{13}C 90° pulse width, and 25 μs 90° pulse width in the ^{1}H WALTZ-16 decoupling sequence. On a sample containing ~8 mM peptide in a bicelle medium it was possible to accumulate a good carbon-13 spectrum in 6−10 h. In cases where suppressing the background ^{13}C signals from the lipids was important, 1D-INADEQUATE experiments were run (*35*). The experimental parameters were the same as for the one-pulse ^{13}C experiments, except that a double quantum filter sequence was inserted, with delays adjusted approximately for the expected size of the couplings, i.e., to $^1/_4(D + J)$.

For ^{15}N spectra, cross polarization (CP) was employed (*36*) with a synchronous WALTZ-8 modulated spin lock on both irradiation channels or an adiabatic tangent ramped CW irradiation on the ^{15}N nucleus (*37*). Typical experimental parameters include a 10 μs hard 90° pulse on proton, followed by a 5.5 kHz CP radiofrequency field (corresponds to a 45 μs 90° pulse) with a typical mixing time of 1 ms. A suitable recycling delay of 2 s was selected on the basis of T_1 measurements of the lipid protons. Typically on an ~8 mM peptide sample it was possible to accumulate a good nitrogen-15 spectrum in 10−24 h. Homonuclear proton decoupling was accomplished by use of a frequency-switched Lee−Goldburg (FSLG) sequence (*38*) implemented on a waveform board capable of 300 ns phase modulation elements.

A two-dimensional separated local field (SLF) experiment was used to measure heteronuclear dipolar couplings from splittings in the indirect dimension. In this experiment the heteronuclear magnetization evolves under the proton spin field in the presence of homonuclear decoupling of protons (*39*, *40*). Typical experimental parameters are 40 t_1 increments, a CP mix of 1 ms with an adiabatic tangential ramp at a 90° pulse width of 45 μs, FSLG homonuclear decoupling during t_1 evolution at a 12.5 kHz field strength, which results in a dwell time of 260 μs (3846 Hz sweep width), and a 25 ms acquisition time under WALTZ-16 proton decoupling at a power level that corresponds to a 90° pulse width of 30 μs.

Analysis of Anisotropic Spin Interactions. The order matrix approach was employed to obtain structural and motional information from the measured anisotropic spin interactions (*41*−*43*). The application of this method has been extensively described in the literature (*25*). Order matrix calculations were performed by the ORDERTEN_SVD C program using the numerical method of singular value decomposition (*44*). If less than three data points were available for a rigid unit this routine was not suitable, because a large three-dimensional null space would have had to be sampled, and the random search version of the ORDERTEN program was used (*26*). The values of the peptide carbonyl ^{13}C and the amide ^{15}N shift tensor elements and the orientation of the shift tensors were based on literature values (*45*, *46*). Since it is known that local structure can influence the chemical

shift tensor elements, an error of ±2 ppm was used, instead of the experimental uncertainty of 0.3−0.5 ppm, for all δ_{an} values in the order matrix calculations.

Order matrix calculations yield a distribution of order parameters ($|S_{z'z'}| > |S_{y'y'}| > |S_{x'x'}|$) and a collection of vectors defining the possible directions of the principal axis frame (PAF). The axis of the PAF that belongs to $S_{z'z'}$ is referred to as the principal order director. To facilitate the visualization of the distributions of vectors, a mapping technique was employed (*26*, *44*, *47*). For maps presented in this paper one of two frames is used: (i) a peptide bond frame for which the carbonyl bond of the amide plane is along the *z* axis and the C−N bond is in the *y*−*z* plane or (ii) a helix frame for which the *z* map axis coincides with the helix axis and the *x* axis points approximately from the helix axis to the carbonyl carbon of Phe_5. In the latter case, a perfect right-handed helix was generated as a model by molecular mechanics minimization methods [all-atom force field of AMBER 4.1 (1995, UCSF)]. Dynamic information is presented as a plot of the largest order parameter ($S_{z'z'}$) versus the asymmetry parameter [$\eta = (S_{x'x'} - S_{y'y'})/S_{z'z'}$].

RESULTS

High-Resolution ^{1}H NMR Spectroscopy. To characterize in a general way the preferred secondary structures of the N-myristoylated and the nonmyristoylated 15 residue peptides, we use high-resolution ^{1}H solution NMR spectroscopy in micelles. Comparison of the one-dimensional ^{1}H spectra of the nonmyristoylated ARF1-15 in water (15% D_2O) and in a DPC micelle solution indicates that the peptide undergoes significant changes and becomes structured upon interaction with the detergent. The change is readily reflected in the increased spectral dispersion of the peptide resonances in the micelle solution. The ARF1-Myr15 peptide's water solubility is very low; thus it was not studied in an aqueous solution, only in micelle solution, but its resonances are similarly dispersed in this medium.

Sequence-specific resonance assignments for the ARF1-Myr15 and the ARF1-15 peptides were based on the observation of sequential NOESY cross-peaks, as proposed by Wüthrich (*30*). First, the spin systems were classified as to amino acid type by the intraresidue amide NH−H^α−H^β (N−α−β) connectivities in the TOCSY spectrum and H^β aromatic proton connectivities in NOESY spectra. The sequential backbone ^{1}H resonance assignments were then made on the basis of identification of the NHNH(*i*, *i* ± 1), H^αNH(*i*, *i* + 1), and H^βNH(*i*, *i* + 1) NOESY cross-peaks. Some overlap of the cross-peaks complicated the analysis, but among backbone resonances only those of Asn_3 could not be assigned, possibly because of fast exchange of the amide proton. A summary of assignments is included as Supporting Information.

The information collected from the NOESY and TOCSY spectra were directly used in determining the secondary structure of the peptides. The H^α,NH(*i*, *i* + 3) and the NHNH(*i*, *i* ± 1) NOE cross-peaks were identified on the basis of the assignment. The sizes of the vicinal spin−spin coupling constants ($^3J_{H\alpha NH}$), which show strong correlation with the intervening torsion angle, and hence secondary structure (*48*, *49*), were qualitatively assessed on the basis of the TOCSY and NOESY data. The H^α chemical shift deviations from the random coil values are also indicative of the secondary structure of a peptide (*50*), with upfield shifts indicating an α-helical structure. On the basis of all the data collected, the ARF1-Myr15 and ARF1-15 peptides are highly helical and they have very similar secondary structures. Accurate identification of the beginning and end of the helices is more complicated. The α chemical shift index and the $^3J_{N\alpha}$ couplings suggest that the helix starts at residue 4 (Ile_4) and ends before Phe_{13}. A summary of sequential and short-range NOEs and chemical shift data, identifying the secondary structure of the peptides, is given in Table 2.

Table 2: Summary of ^{1}H NMR Data for ARF1-Myr15 and ARF1-15

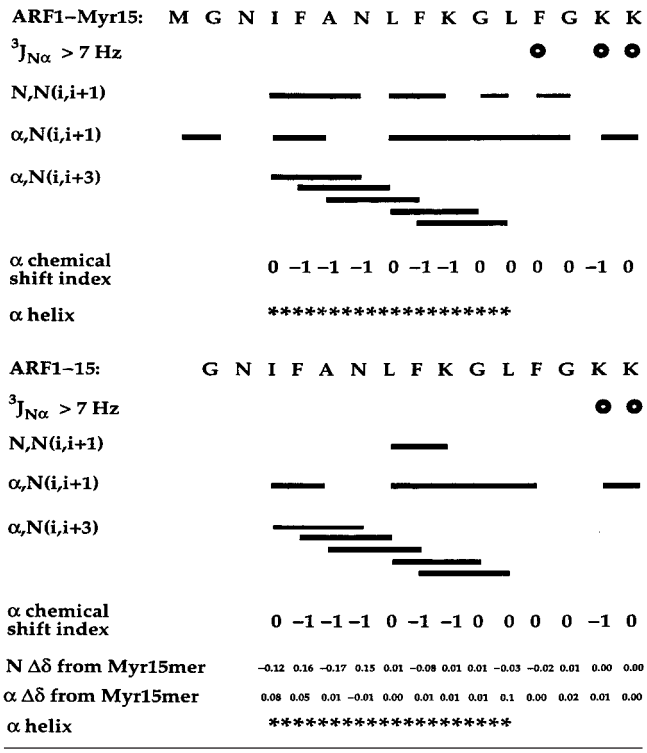

The N-terminal first five amino acids show significant deviation in the amide proton chemical shift between ARF1-Myr15 and ARF1-15, while the H^α shifts are quite similar. This may reflect the fact that the α chemical shift deviations from the random coil values are mainly sensitive to changes in the secondary structure (*50*), while the amide proton chemical shifts are more related to hydrogen-bonding effects and can be very complex (*51*, *52*). For example, it is suggested that an upfield amide proton shift indicates a decrease in the hydrogen bonding of the amide proton with solvent (*53*), but increased hydrogen bonding of the solvent with the backbone carbonyl group results in a downfield shift of the connected amide proton (*54*). Since in an α-helix the carbonyl carbon of residue *n* is hydrogen-bonded to the NH of residue *n* + 4, the first few amide protons in a helix have no intraresidue hydrogen bonds. Thus, the observed differences in the amide proton shifts between ARF1-Myr15 and ARF1-15 for residues 3−6 need not be inconsistent with the existence of an α helix beginning at residue 4; they can simply reflect differences in solvent exposure. It is reasonable to assume that the presence of an N-terminal lipid anchor could influence the extent to which the N-terminal moiety

is buried in the micelle and sequestered from the water without affecting the secondary structure.

High-Resolution ^{13}C NMR in LPC Micelles. High-resolution ^{13}C observe experiments in micelles were mainly carried out to provide a chemical shift reference for the measurement of chemical shift anisotropy offsets, δ_{an}, a useful orientational parameter that has been extensively discussed in the previous study and in the literature (*26*, *55*). However, since ^{13}C shifts in macromolecules appear to primarily reflect the local geometry of atoms that are bonded to the nucleus under study, as opposed to environmental effects (*56*), they may also be used to compare torsion angles of the same amino acid in different sequential positions of a polypeptide chain. LPC micelles were used in these studies, as opposed to the DPC micelles used for the ^{1}H experiments, because the narrow ^{13}C lines and the selective labeling allows us to use larger micelles, which may better approximate bilayer surfaces.

Assignments of the resonances from the phenylalanine rings were easily made based on typical carbon-13 shifts of monosubstituted benzenes, with C_γ furthest downfield and C_ζ furthest upfield (*57*) (see Supporting Information). All three phenylalanine side chains appear very similar in DMSO, but upon interaction with micelles small chemical shift changes occur. The Phe_5 and Phe_9 shifts remain very similar, with C_γ shifting nearly -2 ppm and C_δ, C_ϵ, and C_ζ shifting approximately -1 ppm upon going from DMSO to interactions with lipids. The Phe_{13} resonances shift in the same direction but to a different extent: C_γ only shifts -1 ppm and C_δ only shifts -0.5 ppm.

While interresidue ring-current effects may contribute to shift changes, these effects cannot dominate, because one would expect similar shift changes for directly bonded protons if this were the case; such shifts are not observed. A more likely explanation, at least for shifts of γ and δ carbons, rests on changes in local geometry (torsion angles χ_1 and χ_2) of phenylalanine side chains. Geometries may be similar in DMSO for the three phenylalanine side chains but different once the peptide has formed a helix. Steric interactions with hydrogens usually cause a shielding of the attached carbons (*57*, *58*); thus the upfield shift of the Phe_5 and Phe_9 resonances may indicate that these rings have adopted χ_2 torsion angles that bring phenyl rings into close contact with the backbone of the peptide. Phe_5 and Phe_9, which are in the middle of an amphipathic helix, appear to have very similar local geometry during lipid association, while that of Phe_{13} seems to differ. In the nonmyristoylated ARF1-15 peptide only the phenylalanine residue at position 9 was labeled (ARF1-15-II), but data for this site are comparable to those for Phe_9 of the myristoylated peptide.

Assignments of Spectra in DMPC/DHPC Bicelles. Spectra in field-oriented DMPC/DHPC bicelles allow the measurements of structurally useful parameters from anisotropic spin interactions. Because chemical shift anisotropies often dominate resonance positions in this medium, resonances must be independently assigned. Previously we have reported some assignments for the ARF1-Myr15-I peptide in a bicelle medium. The efforts presented here assign newly labeled sites so that the initial structure of the myristoylated peptide can be further refined. They also correct a previous error in assignment. The new sites include several positions in the backbone that allow observation of ^{15}N as well as ^{13}C. To better understand the importance and role of the lipid anchor, studies include nonmyristoylated forms (ARF1-15) with several of the same labeled backbone and side chain sites.

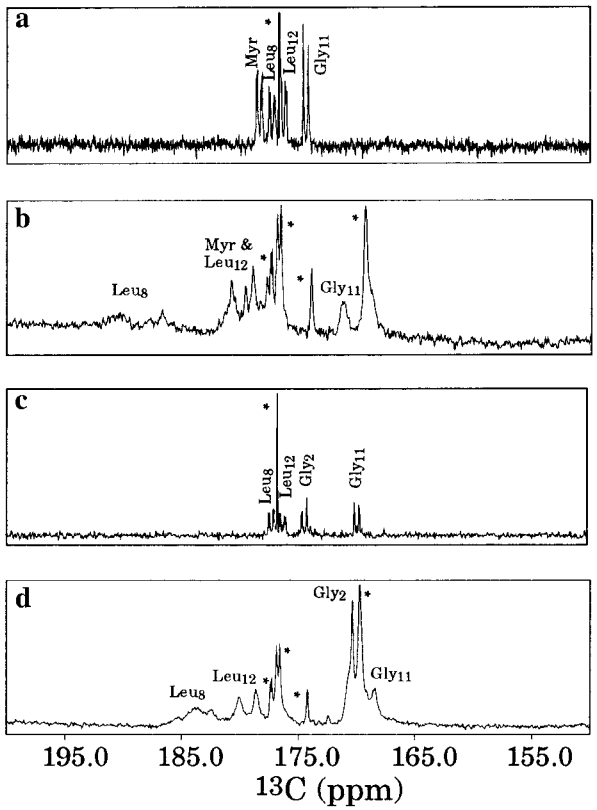

FIGURE 1: Comparison of the isotropic and oriented ^{13}C spectra of the ARF1-Myr15-I and the ARF1-15-I peptides. Only the carbonyl region is shown. (a) Proton-decoupled ^{13}C spectrum of ARF1-Myr15-I in isotropic LPC micelles; (b) proton-decoupled ^{13}C spectrum of ARF1-Myr15-I in magnetically oriented DMPC/DHPC bicelles; (c) proton-decoupled ^{13}C spectrum of ARF1-15-I in isotropic LPC micelles; and (d) proton-decoupled ^{13}C spectrum of ARF1-15-I in magnetically oriented DMPC/DHPC bicelles. Asterisks indicate background lipid signals.

Upon orientation of the bicelles, the peptide resonances become widely dispersed due to chemical shift anisotropy effects (δ_{an}). The splittings of resonances also change, due to the fact that the dipolar interactions no longer average to zero. Figure 1 presents isotropic and oriented ^{13}C spectra of the similarly labeled myristoylated and nonmyristoylated ARF-15-I peptides. The carbonyl region of the spectrum is shown because this exhibits the largest shift dispersion due to chemical shift anisotropy offsets. There are clearly large changes on induction of an orientational preference for both peptides. Comparison of myristoylated and nonmyristoylated spectra, however, reveals a surprisingly high degree of similarity. There is a small difference in extent of shift and the appearance of a resonance assigned to Gly_2 that is not labeled in the myristoylated peptide, but the relative positions for resonances from Leu_8, Leu_{12}, and Gly_{11} are the same. As the spectra in the oriented state are dominated by orientational effects, as opposed to chemical structure, one can speculate that the two peptides adopt similar conformations. To be certain of this similarity, one must systematically assign resonances and measure other orientationally sensitive parameters such as dipolar splittings.

The assignment of the backbone ^{13}C carbonyl resonances of ARF1-15-I can be approached by use of 1D ^{13}C

INADEQUATE spectra. This approach has been extensively discussed in the previous study of ARF1-Myr15 in bicelles (*26*), and only the general procedure and a summary of the results will be presented here. $^{13}C_{\alpha}-^{13}C_{carbonyl}$ connections through double quantum coherence allowed distinction of resonances belonging to leucines as opposed to glycines because of the unique chemical properties of the α-carbons and the ability to pair resonances of these carbons with those for bonded carbonyls by their mutual dipolar coupling. It was possible to assign Gly_2 resonances specifically from the extreme C_{α} chemical shifts and the very narrow line width that is typical for a terminal residue. Distinguishing between the two leucine residues was achieved by use of additional data from ARF1-15-II, a peptide that had only one labeled backbone segment, the $Leu_{12}-Phe_{13}$ amide plane. The new assignments contradict two previously reported assignments of the ARF1-Myr15 peptide, in that assignments of carbonyl resonances for Gly_{11} and Leu_{12} are interchanged. As in the present case, previous assignments had been based on 1D INADEQUATE spectra and used the similarity of coupling sizes to pair carbonyl and α-carbon resonances. Although this experiment is a very powerful tool in assignment of carbonyl ^{13}C resonances, it can fail if some resonances are obscured and if there is an accidental degeneracy in coupling sizes. Unfortunately, this happened for the ARF1-Myr15-I peptide. The Leu_{12} carbonyl resonances were severely overlapped by the Myr carbonyl resonances, the glycine α resonance was broad, and the size of Leu_{12} and Gly_{11} $^1|J + D|_{CC\alpha}$ couplings were comparable. The well-resolved Leu_{12} C_{α} doublet and Gly_{11} carbonyl doublet were incorrectly paired. Synthesis of the ARF1-Myr15-II peptide containing only the labeled Leu_{12} segment allowed observation and correct assignment of the previously obscured carbonyl.

The assignment of the ^{15}N amide resonances can be approached by use of $^{13}CO-^{15}N$ connections once the carbonyl assignments are known. Assignment of the Phe_{13} ^{15}N resonance was, of course, straightforward based on data from ARF1-Myr15-II, which has only this one labeled ^{15}N amide site. Distinction between the amide signals of Phe_9 and Gly_2 in ARF1-Myr15-I could be achieved by comparing the ^{13}C-coupled and the ^{13}C-decoupled ^{15}N spectra (Figure 2), since the $^{13}C-^{15}N$ dipolar couplings for Gly_2 and Phe_{13} had been measured and are quite different.

The ARF1-Myr15-III and ARF1-Myr15-IV peptides were synthesized later in our studies to allow acquisition of information on additional sites along the backbone of the myristoylated peptide. The labeling pattern of these peptides was designed in such a way that assignment would be straightforward. Both peptides had only one ^{13}CO and only two amide ^{15}N sites, out of which $[^{15}N]Leu_8$ was shared between the two so that the common resonance position of $[^{15}N]Leu_8$ in both samples uniquely assigned this residue. The ^{13}C spectra of ARF1-Myr15-III helped to determine the position of the resonance of Ile_4, while the spectra of ARF1-Myr15-IV helped to reconfirm the assignment for ^{13}CO of Gly_{11}. From the ^{15}N spectra of these peptides the resonance position of the amide nitrogens for Phe_5, Leu_8, and Leu_{12} were also determined.

The ^{15}N assignments for nonmyristoylated ARF1-15 were more problematic. The ARF1-15-II peptide, which had only a single ^{15}N label, could again be used as a starting point, establishing that the ^{15}N amide Phe_9 resonance is at 110 ppm.

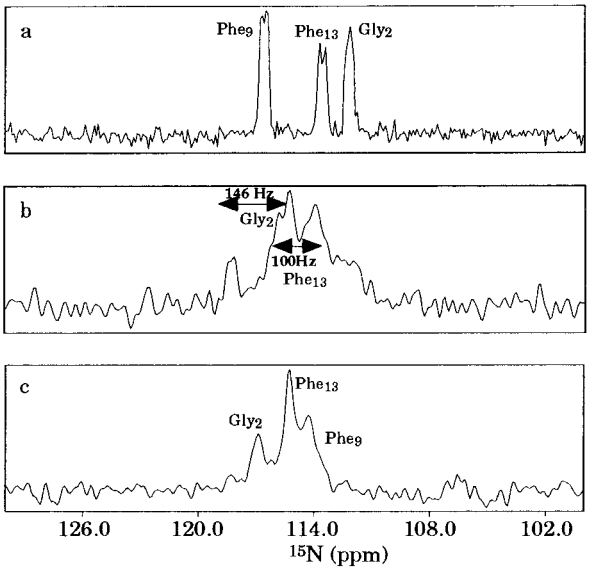

FIGURE 2: Comparison of the (a) ^1H-decoupled ^{15}N spectrum of ARF1-Myr15-I in isotropic micelles to (b) ^1H-decoupled and the (c) ^1H- and ^{13}C-decoupled ^{15}N spectrum of ARF1-Myr15-I in oriented DMPC/DHPC bicelles.

ARF1-15-I had four ^{15}N labels that, in analogy to the myristoylated peptide, one might have expected to be resolved and to show discrete $^{15}N-^{13}C$ couplings. Unfortunately, in proton decoupled spectra, only a single resonance at 110 ppm with a broad shoulder from 110 to 105 ppm could be observed. Only by recording ^1H-coupled spectra by a 2D-SLF technique (*40*), which correlates ^{15}N chemical shift with $^1H-^{15}N$ dipolar coupling, could all four amide resonances be resolved (Figure 3). Phe_{13} could be assigned on the basis of data from ARF1-15-II, which showed this resonance to be at 110 ppm. Another sharp resonance at 110.3 ppm was assigned to Gly_{14} on the basis of its intensity and the fact that resonances from other residues near the C terminus have been sharp. Phe_5 was only 56% ^{15}N-enriched in ARF1-15-I, so it was assigned to the lowest intensity resonance at 106 ppm. Phe_9 is left to account for resonances at 108.5 ppm. While there may be some uncertainly in these assignments, the similarity of chemical shifts and the fact that some dipolar couplings (Phe_9 and Phe_5) are very similar means that exchanging these assignments is not likely to affect the final calculations significantly.

Measurements of Orientational Parameters. The chemical shift assignments described above, when compared to assignments in isotropic medium, give useful orientational information through their dependence on chemical shift anisotropy tensors. These tensors can be defined in coordinate frames fixed to various functional groups, the carbonyl groups of each peptide bond, for example. When the orientation of these groups departs from isotropy, the observed chemical shift changes (δ_{an}) in a way that relates to the preferred orientation. For each labeled carbonyl in the ARF peptides the value of δ_{an} was determined from the chemical shifts measured in micelles as the isotropic value. Use of chemical shift anisotropy offsets to restrict possible orientations of functional groups in trial structures has been described previously (*26*). The new data to be used in this paper are presented in Table 3.

The measurement of splittings of resonances from partially oriented molecules gives another very useful orientational

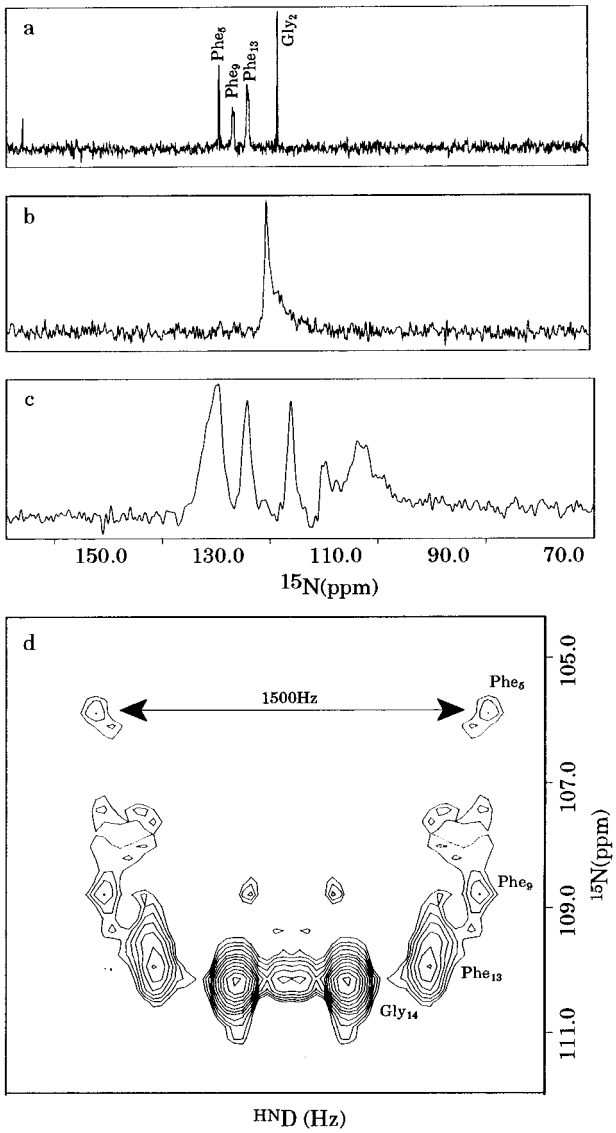

FIGURE 3: Comparison of ARF1-15-I ^{15}N spectra: (a) ^{1}H WALTZ-decoupled spectrum in isotropic micelles; (b) ^{1}H WALTZ-decoupled spectrum in oriented bicelles; (c) ^{1}H homonuclear-decoupled spectrum in oriented bicelles; (d) 2D ^{15}N observed SLF spectrum in oriented bicelles.

constraint through the angular dependence of residual dipolar couplings between bonded pairs of spin $^{1}/_{2}$ nuclei. Again, the use of these data have been discussed previously (*26*). Coupling between $^{15}N-^{1}H$ pairs is among the most easily acquired dipolar information for weakly aligned molecules. However, in molecules strongly anchored to bicelles, strong $^{1}H-^{1}H$ coupling complicates measurement. The frequency-shifted Lee−Goldberg sequence (FSLG) used in collecting the data in Figure 3 was employed to remove $^{1}H-^{1}H$ couplings.

Additional dipolar couplings including $^{13}C-^{13}C$ and $^{13}C-^{15}N$ were acquired as previously presented. A complication that arises in all of the dipolar data is the existence of multiple sign sets; this arises because the sign of the splitting due to residual dipolar coupling cannot normally be directly measured, and one must consider both sign possibilities with scalar coupling either adding or subtracting to generate the measured value for directly bonded pairs. Yet, reduction in the number of possible sign sets would greatly add to the utility of the data in definition of allowed structures. In cases where sufficient data exist for a single amide plane, one often finds that only one set will allow a description in terms of a general order matrix. Some of the possible sign sets were eliminated on this basis. Table 3 summarizes and compares all the collected orientational data for the backbone of the ARF1-Myr15 and the ARF1-15 peptides, including both new data and previously analyzed ^{13}C data.

DISCUSSION

In our previous study of a myristoylated ARF fragment we were able to conclude that the myristoylated peptide, when associated with a bilayer, was predominantly helical, with the helix axis nearly parallel to the bilayer surface (*26*). The parallel orientation was most strongly supported by data for the Leu_8-Phe_9 amide bond, where numbers of measurements were sufficient to independently determine a preferred orientation. Data for the $Gly_{11}-Leu_{12}$ bond were merely consistent with a helical model, and data for the $Leu_{12}-Phe_{13}$ bond indicated that the helix terminated prior to this bond. Data were insufficient for a more complete analysis of either structural or motional properties of the membrane-bound state. Our initial objectives for the current paper were, therefore, to acquire the additional data needed for this more complete analysis and to investigate structural or motional alterations associated with the removal of the N-myristoyl group. The discovery in the course of the studies that carbonyl shift data for the $Gly_{11}-Leu_{12}$ and $Leu_{12}-Phe_{13}$ bonds had been interchanged due to an assignment error in the previous studies provided additional motivation for a more complete analysis. By combining high-resolution data on the secondary structures of the peptides with additional orientational data in bicelle medium, we are now able to present a single helical model that allows a description of motional averaging among bilayer association modes. Moreover, we are able to show that while the myristoyl chain may increase bilayer association tendency, it does not greatly affect the mode of association or preferred conformation of the peptide.

Orientational Analysis of Individual Peptides. Analysis of the measured anisotropic spin interactions, dipolar couplings, and chemical shift anisotropy data is based on an order matrix approach (see Materials and Methods). In general, five independent pieces of data are needed from a rigid fragment for an unambiguous evaluation of the order matrix. When this is possible, the order matrix can be diagonalized to define the direction of a principal order frame as seen from the point of view of the fragment and to define the principal order parameters [$S_{z'z'}$ and an asymmetry parameter $\eta = (S_{x'x'} - S_{y'y'})/S_{z'z'}$). Since order is dictated by association with the oriented bicelle system, the direction of the principal order frame axes defines peptide orientation relative to the bicelle surface. The magnitudes of the principal order parameter and asymmetry parameter define amplitudes of motion. When principal order parameters of different fragments are very similar, an argument can be made for participation of these fragments in a single rigid model for the molecule under study. The molecular model can then be generated by reorienting fragments so their principal order frames coincide.

In practice, because of experimental limitations, one seldom achieves the goal of making sufficient independent measurements, using only the atoms of the minimal rigid

Table 3: Summary of Anisotropic Spin Interaction Data for the Backbone of ARF1-Myr15 and ARF1-15 Peptides[a]

	δ_{an} (^{13}C)	δ_{an} (^{15}N)	$^1D_{CC}$	$^1D_{CN}$	$^1D_{NH}$
Myr	+1.0[b]		−283 or +177 ± 20[b]	−135 or +165 ± 30[b]	< |500|
Gly_2		+4.75			
	+0.2		−233 or +127 ± 20		
Asn_3					
Ile_4	+6.8			−180 or +208 ± 30	
Phe_5		−4.2			−790 or +1120 ± 300
		−13.0			−2300 or +2700 ± 300
Ala_6					
Asn_7					
Leu_8	+11.5[b]	−3.2	−330 or +224 ± 200[b,c]		
	+6.4				
Phe_9		−2.4			
		−9.0			−2300 or +2700 ± 300
Lys_{10}					
Gly_{11}	−4.0 (+4.5[b])		−323 or +217 ± 50[b]		
	−5.4		−353 or +247 ± 50		
Leu_{12}	+2.5 (−7.6[b])	−3.5	−310 or +210 ± 20[b]	+15 ±20	< |400|
	+2.9		−240 or +142 ± 20		
Phe_{13}		+2.5		−81 or +111 ± 20[b]	−600 or +950 ± 300
		−3.6		+15 ±20	−1500 or +1800 ± 300
Gly_{14}					
		+2.1			−460 or +790 ± 100

[a] For each residue, the first row is for ARF1-Myr15 and the second row is for ARF1-15. [b] Previously reported data (*26*). All couplings are in hertz, and the anisotropic part of the chemicals shifts are in parts per million. [c] The previously reported value of $^1D_{CC}$ of Leu_8 has been scaled to match the bilayer order used in current studies.

unit, i.e., atoms of a single peptide plane, to unambiguously determine an order matrix. Of the five amide planes examined in this new study, there are three cases for which sufficient experimental data were acquired to position a peptide bond with respect to the bilayer with some accuracy. These are the amide bonds between Ile_4 and Phe_5, Leu_8 and Phe_9, and Gly_{11} and Leu_{12}. For the Ile_4-Phe_5 and $Gly_{11}-Leu_{12}$ amide planes only four data points were actually measured. However, because of some unique positioning of interaction vectors only one possible sign set gave order matrix solutions in each case, and principal order frames and order parameters were moderately well determined. Figure 4 shows both the directions of allowed frames and the allowed order parameters for the Ile_4-Phe_5 and $Gly_{11}-Leu_{12}$ bonds. We focus on these because the data on these bonds are new; the orientation of the Leu_8-Phe_9 bond was previously characterized and has an orientation consistent with new ^{15}N shift offset data reported here. However, we will not attempt to directly combine old and new data in our calculations because of difficulties in reproducing levels of order for various samples. The fragment frame in each case is chosen so that the *z* axis is along the C−O carbonyl bond and the amide plane is in the *y*−*z* plane. In the Sauson−Flamsteed projections at the left of the figure, the *z* axes are at the apexes of the plots and the *x* axes point out from the centers of the plots. One can see that the allowed directions of most order (black dots most positive and gray dots most negative) are in both cases clustered about the equator of the projection diagrams. Assuming that the direction of highest order is coincident with the bilayer normal, this is consistent with both carbonyls pointing in a direction approximately parallel to the bilayer surface. The plots of order and asymmetry parameters at the right of Figure 4 show a wide range of possible values. These ranges become more restricted once fragments are combined in a unified model.

For the amide planes close to the N and the C terminus ($Myr-Gly_2$ and $Leu_{12}-Phe_{13}$) it was possible to determine five orientational data points, but these lead to numerous possible sign sets for dipolar coupling and multiple orientation solutions. In the case of ARF1-15 the amide planes were also less well determined. Out of the five studied fragments, only the one between $Leu_{12}-Phe_{13}$ had enough labeled sites to measure five independent data points; for the other amide planes typically only two data points could be collected. We therefore defer a discussion of data on the nonmyristoylated peptide to an approach that views them in a more structurally unified context.

Analysis Based on an Intact Helix. On the basis of an analysis of high-resolution ^{1}H NMR data measured in nonoriented micellar solutions, it could be concluded that the myristoylated and the nonmyristoylated peptides have a very similar secondary structure, with an α-helical segment between residues 4 and 12. Assuming that this α-helix is rigid (i.e., the positions of the amide planes do not change with respect to each other over the time scale of NMR dipolar couplings), it is possible to take the order matrix calculations one step further by combining all anisotropic spin interactions for the Ile_4-Leu_{12} segment. This gives 7 δ_{an} and 5 D_{ij} values for the helical unit considered as a single fragment, now an overdetermined system. By combining all the available data from residues 4−12 of the peptide it was still possible to obtain acceptable order matrix solutions, confirming that these residues can share a common order matrix. In these order matrix calculations, error values were increased by a factor of 1.5 to account for possible imperfections in the assumed α-helical structure. Out of 10 000 cycles, 1303 gave acceptable order matrix solutions. Figure 5a shows the resulting possible orientations of the principal averaging frame, as well as the distribution of the order parameters. It should be noted that now the solutions are tightly clustered, defining the orientation of the helix with respect to the magnetic field to high accuracy and giving better defined ranges for principal order and asymmetry parameters. Here, the long axis of the helix has been assigned as the *z* axis,

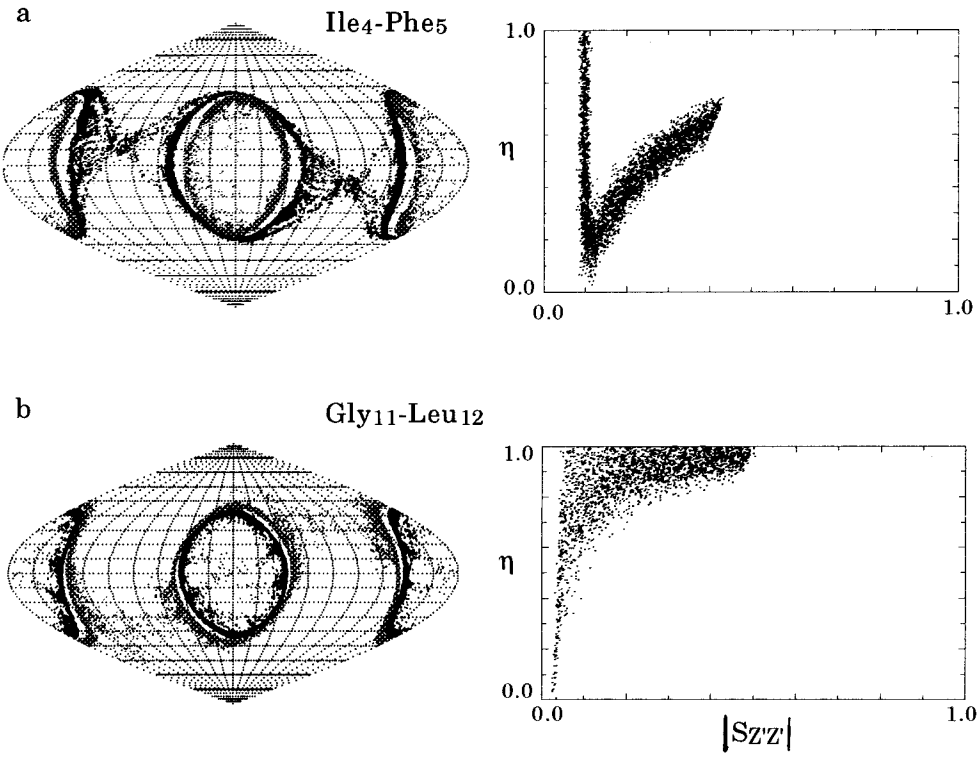

FIGURE 4: Results of the order matrix calculations for the midhelix amide planes. Sauson−Flamsteed projections show the directions of the principal averaging frames and the $S_{z'z'}$ vs η plots show the level of order. (a) Ile_4-Phe_5; (b) $Gly_{11}-Leu_{12}$. The mapping frame has the carbonyl bond along the z axis. Black dots indicate the direction of the axis with the largest positive order parameter (outer ring for Ile_4-Phe_5 and inner ring for $Gly_{11}-Leu_{12}$), and gray dots indicate the direction of the axis with the largest negative order parameter.

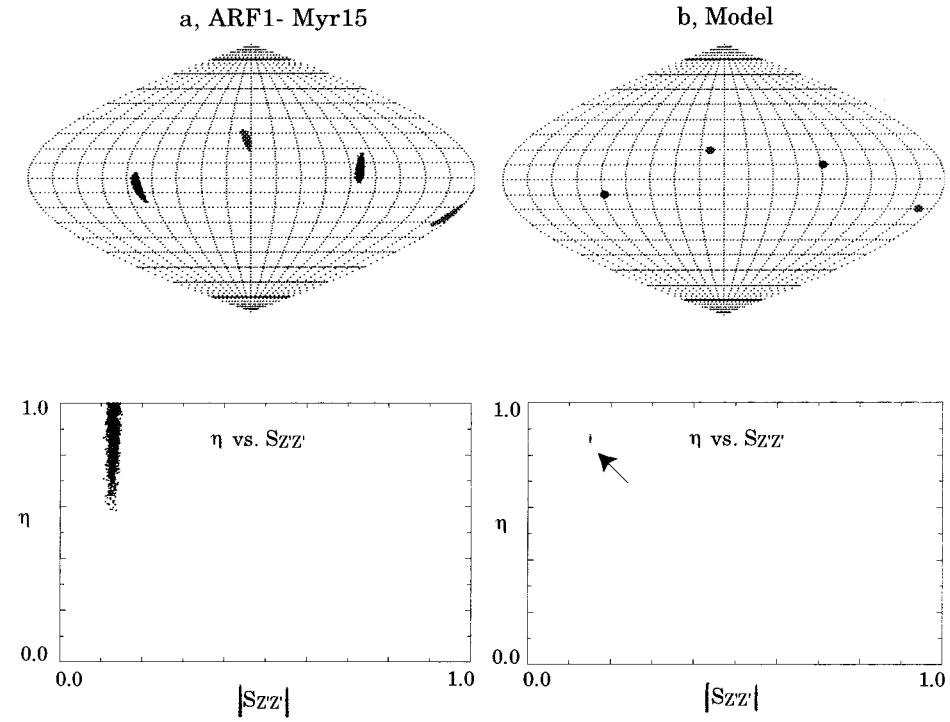

FIGURE 5: Results of the order matrix calculations for the helical segment of ARF-Myr15. Sauson−Flamsteed projections show the directions of the principal averaging frames and the $S_{z'z'}$ vs η plots show the level of order. The mapping frame has the helix axis along the z axis. Black dots indicate the direction of the axis with the largest positive order parameter, and gray dots (near center of map) indicate the direction of the axis with the largest negative order parameter. (a) Solutions based on experimental data; (b) solutions based on the two-state model.

and dots again show the direction of the most ordered axes. The highest level of absolute order in this case is represented primarily by the gray dots. The principal order axis defined by these dots is nearly perpendicular to the helix.

It is known that bicelles orient with their normal perpendicular to the magnetic field, so if a molecule is associated with the bilayer surface (as opposed to bicelle edge), one would expect a negative principal order parameter (Figure

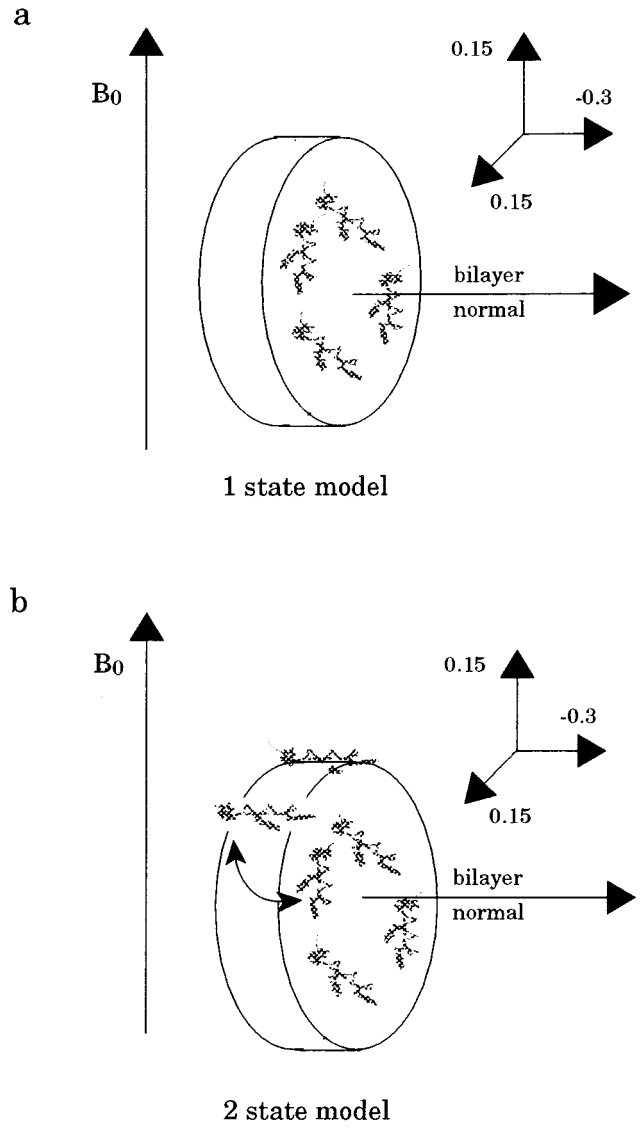

FIGURE 6: Possible models of peptide−bicelle interactions. (a) Model with the peptide being associated only with the bicelle face: one-state model. (b) Model with the peptide being associated with both the face and the edge of the bilayer disk: two-state model. The axis systems show the directions and values of order parameters that pertain to each state for the associated peptides.

6a). We would also expect the most ordered direction to be along the bilayer normal and perpendicular to the helix axis if the helix orients parallel to the bilayer surface (actually we find the axis to be about 20° off perpendicular for most solutions). Note that the most negative ordered axis is also nearly along the initial *x* axis of the helix. This is a direction that would allow the most hydrophobic groups to associate with, or insert into, the bilayer surface. With the principal alignment frame now identified, we redefine the axis with the most negative order parameter as the z' axis and the axis with the most positive order parameter as the y' axis.

The data indicate some deviation from the very simple picture given above in that the asymmetry parameter is not near zero ($\eta = 0$ for axial symmetry). One might have expected a peptide with a single mode of association with the bilayer surface to reflect the axial symmetry of the bilayer. Let us consider the nature of motion that could lead to asymmetry. Any anisotropic motions executed by the peptide relative to the bilayer surface could produce this effect; for example, rolling of the helix from side to side while it lay on the surface. However, such rolling would leave the order parameter for the helix axis (now $S_{x'x'}$) unchanged and scale down $S_{z'z'}$ and $S_{y'y'}$. This is not what happens; it is $S_{x'x'}$ that is scaled down, so there must be a motion that is in effect a rotation about the new y' axis. One type of motion that averages the order along the helix axis and an axis that is perpendicular to the helix, while leaving the third axis, which is parallel to the bilayer surface, unchanged is a flip-flop between bilayer surface association and bicelle edge association. We will call this the two-state model (Figure 6b).

An additional result of the motion depicted in Figure 6b would be that the bicelles's and the peptide's principal order directors no longer coincide. Displacement from the orientation perpendicular to the helix axis, expected for the two-state model, depends on the extent of the rotation and the population of the rotation states. It is possible to reproduce the ARF1-Myr15 results with good precision with a rotation of $\lambda = 80°$ and a population of 2:1 surface:edge. The rotation axis is 10° off the *y* axis in the $z-y$ plane of the initial molecular frame. Figure 5b illustrates the orientation of the principal order axes for the above-described motional model. Calculations were carried out assuming that the bicelle's principal order parameter is −0.3 and that the bicelle is axially symmetric, i.e., $\eta = 0$. The −0.3 value was chosen on the basis of a measured S_{bilayer} that approaches 0.6 for the bicelles used and by taking into account the −0.5 scaling factor that results from the perpendicular orientation of the bicelles. The experimentally available anisotropic spin interactions were predicted by calculating them at both helix orientations and then averaging them according to the relative population of the two states. These data were then used in an order matrix calculation giving the principal averaging frame and the order parameters. As seen in Figure 5, there is good agreement with parameters derived from the experimentally determined order tensor. This two-state model is, of course, not unique, and other descriptions of geometry and motion may also fit the data. It is, however, interesting to note that geometric models for bicelles of the composition used have approximately a 2:1 edge:face surface area ratio, the ratio we would have chosen to use in our calculation if we assumed equal affinities of peptides for faces and edges of bicelles.

With a model for the central part of the peptide helix of ARF1-Myr15 in hand, it is possible to return to the less well-defined terminal residues and side chains. First, we will focus on the C-terminal $Leu_{12}-Phe_{13}$ amide plane. Data for this plane gave a wide range of solutions, especially because of the two different sign sets yielding solutions. However, it was still not possible to fit the data from this amide plane with the same η and $S_{z'z'}$ values as the helix itself, if only rigid structures created by rotation about ϕ and ψ of Leu_{12} are allowed. This is hardly surprising, since we might well expect some internal motions of terminal residues relative to the central helix. Internal motion does not necessarily prevent us from describing an average geometry or using the behavior of the helix to place restrictions on terminal residue order matrix solutions. If the central and terminal segments share the same overall motions, but the terminal residues experience additional axially symmetric internal motions, the order parameters of the terminal segment would

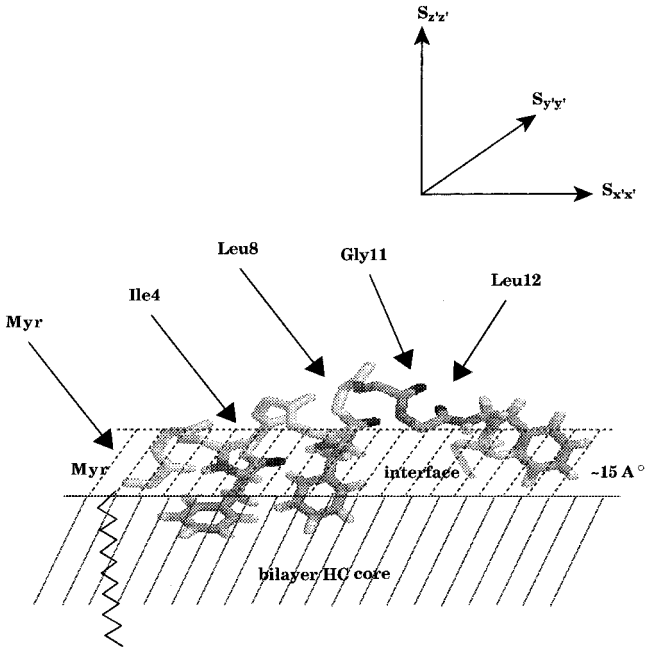

FIGURE 7: Orientation and structure of ARF1-Myr15 at the bilayer surface that is consistent with experimental data.

simply be scaled down; the principal frame orientation and the η values of the two segments would still be the same. If the rigid units experience different asymmetric motions, their order tensors can deviate more severely. However, only large-scale motions can accomplish this (Al-Hashimi and Tolman, personal communication). Thus, the axes of the principal averaging frames of the various rigid fragments may be aligned to yield relative average orientations in most circumstances. Moreover, we can place additional restrictions on solutions for the terminal residue by insisting that its principal order parameter, $S_{z'z'}$, be less than or equal to that of the central helix, and we can insist that its η values fall in the same range.

Thus, in seeking a structural representation for the $Leu_{12}-Phe_{13}$ peptide plane, we restricted the principal order parameter, $|S_{z'z'}|$, to be less than 0.15 and η to be larger than 0.6. Under the above assumptions it was possible to reduce the number of acceptable sign sets from two to one. The results suggest that the carbonyl bond of this amide plane is 30−60° off the helix axis with only slightly smaller principal order parameters. The data from the $Myr-Gly_2$ amide plane was extensively analyzed previously (*26*), and even after considering the newly established two-state model, the conclusion that the carbonyl bond of the $Myr-Gly_2$ amide plain is close to being along the helix axis remains valid.

Although we collected orientational constraints on phenylalanine side chains, the data are not sufficient at this point for an order tensor analysis. We therefore confine our comments about side-chain geometry to ones based on high-resolution chemical shift trends. Comparison of the isotropic ^{13}C shifts from the phenylalanine side chains show that χ_2, and possibly χ_1, torsion angles of the two midpeptide aromatic side chains are similar, while those for Phe_{13} differ when the peptide is in contact with phospholipids. Examining a helical wheel for the peptide may provide some insight into the reasons for these deviations. The hydrophobic side chains of Ile_4, Phe_5, Leu_8, Phe_9, and Leu_{12} can all fit on one side of the helix, but Phe_{13}, if it were part of a helix, begins to push the limits of a single hydrophobic side. Adoption of an alternate conformation is very likely to result. Figure 7 shows a structure for ARF1-Myr15 in the membrane environment that is consistent with all the observed data

Comparison of Myristoylated and Nonmyristoylated Peptides. It was also possible to model the helix for the ARF1-

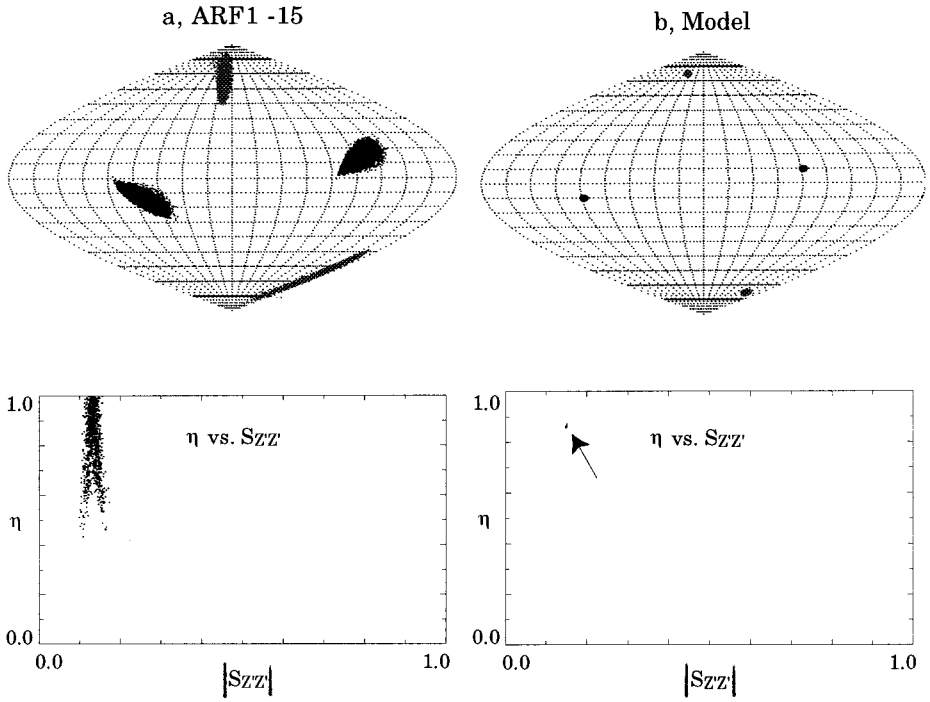

FIGURE 8: Results of the order matrix calculations for the helical segment of ARF1-15. Sauson−Flamsteed projections show the directions of the principal averaging frames and the $S_{z'z'}$ vs η plots show the level of order. The mapping frame has the helix axis along the *z* axis. Black dots indicate the direction of the axis with the largest positive order parameter, and gray dots (near apex of map) indicate the direction of the axis with the largest negative order parameter. (a) Solutions based on experimental data; (b) solutions based on the two-state model.

15 peptide by combining orientational data for the helical segment identified in high-resolution NMR studies. The combined data for residues 4−12 gave three dipolar couplings and four δ_{an} data points. The calculations resulted in 5311 acceptable order matrixes from 10 000 trials. Figure 8a shows the resulting possible orientations of the principal averaging frame. Although the solutions are reasonably tightly clustered, the distribution is less tight than the one determined for ARF1-Myr15 as a result of having fewer orientational constraints.

The direction of this peptide's principal order director, the director with the largest negative order parameter, is severely (∼70°) tilted out of the $x-y$ plane of the helix fixed coordinate system, a result inconsistent with a one-state model in which the helix lies perfectly parallel to the bicelle surface. However, while the directions for the axes with the largest negative order parameters differ radically for ARF1-Myr15 and ARF1-15, the axes with the largest positive order parameter are reasonably close to each other. These axes are also close to being perpendicular to the helix axis and the vector pointing to the most hydrophobic surface. This suggests that a two-state model might play a role in explaining the differences; both peptides switch between orientations by rotation about this most common axis, but distributions between the two states might be different. The ARF1-15 results could be well reproduced by the two-state model with the population ratio of 1:2 surface:edge (Figure 8b). It is not unreasonable to think that, in the absence of a myristoyl chain, peptides might more strongly prefer edge association.

Outside of differences in association, addition of the myristoyl chain did not appear to produce large changes in the structure of the peptide. On the basis of high-resolution data, the extent of the central helical segment is very similar. The peptides did show differences in their N-terminal segments, suggesting that N-myristoylation reduces the solvent exposure of nearby residues, but these differences are minor. Data on the positioning of the $Leu_{12}-Phe_{13}$ peptide plane is also seen to deviate by a small amount. It is interesting that a recent study of a segment of another protein, the E3−13.7 protein, with and without an N-terminal myristoyl anchor in a micelle environment, showed similar results in that no significant change in peptide structure resulted upon myristoylation (*59*).

Conclusions. Thus, we have been able to build a fairly detailed picture of the structural and membrane association properties of both myristoylated and nonmyristoylated peptides derived from the N-terminal helix of ARF1. The propensity of the peptide to remain helical and associate with a bilayer surface, with or without the myristoyl chain, is of potential value in building an understanding of how the ARF1 protein associates with a membrane. It has previously been proposed that this segment remains helical in its association with a membrane (*18*), and we can experimentally support this suggestion. It has also been suggested that the N-terminal helix might extend further than residue 11 (its termination in the nonmyristoylated crystal structure of the soluble GDP form of the protein) when associated with the membrane, making it possible for Phe_{13} to be part of the peptide−membrane hydrophobic interface (*18*). We can support this suggestion to the $Gly_{11}-Leu_{12}$ amide plane. However, there is no inherent tendency to extend the helix to the $Leu_{12}-Phe_{13}$ peptide bond in our peptides. A definitive description of the extent of this helix in a GTP-loaded, membrane-associated form of ARF1 must, of course, await studies with the intact protein. It is hoped that some methods analogous to those presented here will be applicable to such systems in the future.

ACKNOWLEDGMENT

We thank Hashim M. Al-Hashimi and Dr. Mark W. F. Fischer for stimulating discussions on order matrix calculations. We also thank Lilian Fisher for all her advice and for her help with the peptide synthesis.

SUPPORTING INFORMATION AVAILABLE

A table showing chemical shift assignments for the peptides in isotropic micellar solutions. This material is available free of charge via the Internet at http://pubs.acs.org.

REFERENCES

1. Bhatnagar, R. S., and Gordon, J. I. (1997) *Trends Cell Biol. 7*, 14−21.
2. Silvius, J. R. (1999) *J. Liposome Res. 9*, 1−19.
3. Gordon, J. I., Duronio, R. J., Rudnick, D. A., Adams, S. P., and Goke, G. W. (1991) *J. Biol. Chem. 266*, 8647−8650.
4. McLaughlin, S., and Aderem, A. (1995) *Trends Biochem. Sci. 20*, 272−276.
5. Takasaki, A., Hayashi, N., Matsubara, M., Yamauchi, E., and Taniguchi, H. (1999) *J. Biol. Chem. 274*, 11848−11853.
6. Kahn, R. A., and Gilman, A. G. (1984) *J. Biol. Chem. 259*, 6228−6234.
7. Tanaka, T., Ames, J., Harvey, T., Stryer, L., and Ikura, M. (1995) *Nature 376*, 444−447.
8. Geyer, M., Munte, C. E., Schorr, J., Kellner, R., and Kalbitzer, H. H. (1999) *J. Mol. Biol. 289*, 123−138.
9. Sankaram, M. B. (1994) *Biophys. J. 67*, 105−112.
10. Struppe, J., Komives, E. A., Taylor, S. S., and Vold, R. R. (1998) *Biochemistry 37*, 15523−15527.
11. Victor, K., and Cafiso, D. S. (1998) *Biochemistry 37*, 3402−3410.
12. Qin, Z., and Cafiso, D. S. (1996) *Biochemistry 35*, 2917−2925.
13. Rothman, J. E., and Wieland, F. T. (1996) *Science 272*, 227−234.
14. Boman, A. L., and Kahn, R. A. (1995) *Trends Biochem Sci. 20*, 147−150.
15. Franco, M., Chardin, P., Chabre, M., and Paris, S. (1993) *J. Biol. Chem. 268*, 24531−24534.
16. Franco, M., Chardin, P., Chabre, M., and Paris, S. (1995) *J. Biol. Chem. 270*, 1337−1341.
17. Kahn, R. A., Randazzo, P., Serafini, T., Weiss, O., Rulka, C., Clark, J., Amherd, M., Roller, P., Orci, L., and Rothman, J. E. (1992) *J. Biol. Chem. 267*, 13039−13046.
18. Amor, J. C., Harrison, D. H., Kahn, R. A., and Ringe, D. (1994) *Nature 372*, 704−708.
19. Goldberg, J. (1998) *Cell 95*, 237−248.
20. Paris, S., BeraudDufour, S., Robineau, S., Bigay, J., Antonny, B., Chabre, M., and Chardin, P. (1997) *J. Biol. Chem. 272*, 22221−22226.
21. Franco, M., Chardin, P., Chabre, M., and Paris, S. (1996) *J. Biol. Chem. 271*, 1573−1578.
22. Antonny, B., Beraud-Dufour, S., Chardin, P., and Chabre, M. (1997) *Biochemistry 36*, 4675−4684.
23. Opella, S. J., Kim, Y., and McDovell, P. (1994) *Methods Enzymol. 239*, 536−560.
24. Henry, G. D., and Sykes, D. B. (1994) *Methods Enzymol. 239*, 515−535.
25. Sanders, C. R., Hare, B. J., Howard, K. P., and Prestegard, J. H. (1994) *Prog. NMR Spectrosc. 26*, 421−444.

26. Losonczi, J. A., and Prestegard, J. H. (1998) *Biochemistry 37*, 706−716.
27. Chang, C., Waki, M., Ahmad, M., Meienhofer, J., Lundell, E. O., and Haug, J. D. (1980) *Int. J. Pept. Protein Res. 15*, 59−66.
28. Sorensen, R. M., Bodenhausen, O. W., Wagner, G., Ernst, R. R., and Wuthrich, K. (1983) *Biochem. Biophys. Res. Commun. 117*, 479−485.
29. Bax, A., and Davis, D. G. (1985) *J. Magn. Reson. 65*, 355−360.
30. Wüthrich, K. (1986) *NMR of proteins and nucleic acids*, Wiley, New York.
31. Piotto, M., Saudek, V., and Sklenar, V. (1992) *J. Biomol. NMR 2*, 661−665.
32. Wishart, D. S., Bigam, C. G., Yao, J., Abildgaard, F., Dyson, H. J., Oldfield, E., Markley, J. L., and Sykes, B. D. (1995) *J. Biomol. NMR 6*, 135−140.
33. Howard, K. P., and Opella, S. J. (1996) *J. Magn. Reson., Ser. B 112*, 91−94.
34. Losonczi, J. A., and Prestegard, J. H. (1998) *J. Biomol. NMR 12*, 447−451.
35. Shaka, A. J., and Freeman, R. (1983) *J. Magn. Reson. 51*, 169−173.
36. Mehring, M. (1976) in *NMR basic principles and progress* (Diehl, P., Fluck, E., and Kosfeld, R., Eds.) Springer-Verlag, Berlin, Heidelberg, and New York.
37. Hediger, S., Meier, B. M., Kurur, N. D., Bodenhausen, G., and Ernst, R. R. (1994) *Chem. Phys. Lett. 223*, 283−288.
38. Bielecki, A., Kolbert, A. C., and Levitt, M. H. (1989) *Chem. Phys. Lett. 155*, 341−346.
39. Hester, R. K., Ackerman, L. J., Cross, V. R., and Waugh, J. S. (1975) *Phys. Rev. Lett. 34*, 993−995.
40. Hester, R. K., Ackerman, J. L., Neff, B. L., and Waugh, J. S. (1976) *Phys. Rev. Lett. 36*, 1081−1083.
41. Saupe, A. (1968) *Angew. Chem., Int. Ed. Engl. 7*, 97.
42. Diehl, P., and Khetrapal, C. L. (1969) *NMR: basic principles and progress*, Vol. 1, Springer-Verlag, New York.
43. Emsley, J. W., and Lindon, J. C. (1975) *NMR spectroscopy using liquid crystal solvents*., Pergamon Press, Oxford, U.K.
44. Losonczi, J. A., Andrec, M., Fischer, M. W. F., and Prestegard, J. H. (1999) *J. Magn. Reson. 138*, 334−342.
45. Duncan, T. M. (1987) *J. Phys. Chem. Ref. Data 16*, 125−151.
46. Oas, T. G., Hartzell, C. J., McMahon, T. J., Drobny, G. P., and Dahlquist, F. W. (1987) *J. Am. Chem. Soc. 109*, 5956−5962.
47. Bugayevskiy, L. M., and Snyder, J. P. (1995) *Map projections*, Taylor & Francis, London.
48. Karplus, M. (1959) *J. Chem. Phys. 30*, 11−15.
49. Karplus, M. (1963) *J. Am. Chem. Soc. 85*, 2870−2871.
50. Wishart, D. S., Sykes, B. D., and Richards, F. M. (1992) *Biochemistry 31*, 1647−1651.
51. Zhou, N. E., Zhu, B.-Y., Sykes, B. D., and Hodges, R. S. (1992) *J. Am. Chem. Soc. 114*, 4320−4326.
52. Merutka, G., Dyson, H. D., and Wright, P. E. (1995) *J. Biomol. NMR 5*, 14−24.
53. Urry, D. W., and Long, M. M. (1976) *CRC Crit. Rev. Biochem. 4*, 1−45.
54. Llinas, M., and Klein, M. P. (1975) *J. Am. Chem. Soc. 97*, 4731−4737.
55. Cross, T. A., and Opella, S. J. (1994) *Curr. Opin. Struct. Biol. 4*, 574−581.
56. Case, D. A. (1998) *Curr. Opin. Struct. Biol. 8*, 624−630.
57. Breitmaier, E., and Voelter, W. (1987) *Carbon-13 NMR spectroscopy*, VCH, New York.
58. Grant, D. M., and Cheney, V. B. (1967) *J. Am. Chem. Soc. 89*, 5315.
59. Vinogradova, O., Carlin, C., Sonnichsen, F. D., and Sanders, C. R. (1998) *J. Biol. Chem. 273*, 17343−17350.

BI9923050